

Local Electronic Structure and Dynamics of Muon-Polaron Complexes in Fe₂O₃

M. H. Dehn,^{1,2,3,*} J. K. Shenton,^{4,*} D. J. Arseneau,³ W. A. MacFarlane,^{2,3,5}
G. D. Morris,³ A. Maigné,² N. A. Spaldin,⁴ and R.F. Kiefl^{1,2,3}

¹*Department of Physics and Astronomy, University of British Columbia, Vancouver, BC V6T 1Z1, Canada*

²*Stewart Blusson Quantum Matter Institute, University of British Columbia, Vancouver, BC V6T 1Z4, Canada*

³*TRIUMF, Vancouver, BC V6T 2A3, Canada*

⁴*Department of Materials, ETH Zurich, CH-8093 Zürich, Switzerland*

⁵*Department of Chemistry, University of British Columbia, Vancouver, BC, V6T 1Z1, Canada*

(Dated: January 25, 2021)

We perform detailed muon spin rotation (μ SR) measurements in the classic antiferromagnet Fe₂O₃ and explain the spectra by considering dynamic population and dissociation of charge-neutral muon-polaron complexes. We show that charge-neutral muon states in Fe₂O₃, despite lacking the signatures typical of charge-neutral muonium centers in non-magnetic materials, have a significant impact on the measured μ SR frequencies and relaxation rates. Our identification of such polaronic muon centers in Fe₂O₃ suggests that isolated hydrogen (H) impurities form analogous complexes, and that H interstitials may be a source of charge carrier density in Fe₂O₃.

The semiconducting transition metal oxide (TMO) α -Fe₂O₃ [1–3] is a prototypical antiferromagnet whose magnetic properties are still actively studied [4–7]. It is also a promising photoanode for solar water splitting [8–10] due to its natural abundance, non-toxicity and 2.1 eV bandgap that allows for efficient visible light absorption. However, photoelectric device performance is significantly hindered by the formation of small polarons: excess electrons localize on Fe ions and cause both a change in valence from Fe³⁺ to Fe²⁺ and a local lattice distortion [10–13]. As a result, conduction occurs via thermally activated polaron hopping [14–18] rather than efficient band-type transport. Efforts are being made to improve device performance by studying the impact of dopants such as Sn, Ti and Si on polaron transport [17–20], however, little consideration is given to *unintentional* dopants such as hydrogen (H). Incorporated during growth and post-processing, H is one of the most ubiquitous impurities in semiconductors [21–23], and can significantly influence their electronic properties. Since isolated H is extremely hard to study directly, most information about its dopant characteristics comes from the study of muonium (Mu= $[\mu^+e^-]$), a light H analog with virtually identical electronic structure, which is experimentally accessible via the muon-spin-rotation (μ SR) technique [24–27]. Recent μ SR studies reported polaronic Mu centers in non-magnetic TMOs such as SrTiO₃ and TiO₂ [28–30], in which an oxygen-bound, positive muon and a small polaron located on a neighboring TM ion form an overall charge-neutral complex, suggesting that isolated H defects form analogous H-polaron centers. Recently, muon-polaron complexes have been shown to exist in the antiferromagnet Cr₂O₃ [31]. In a crucial distinction to non-magnetic TMOs however, the excess electron spin strongly couples to the unpaired d electrons of the Cr host, resulting in a μ SR signal that is difficult to distinguish from the usual signal of the positive charge state (i.e. the bare muon), and thus may be

easily misidentified. Therefore, “hidden” charge-neutral muon states need to be carefully considered when using the muon as a sensitive local probe of magnetism in insulating magnets, especially TMOs [32, 33].

Here we report a detailed μ SR study on α -Fe₂O₃ and identify, supported by density functional theory (DFT), several muon-polaron complex configurations that are very close in energy. Expanding on early work [34–40], we are able to consistently interpret the complicated μ SR spectra at low temperatures (T) in terms of transitions between various complex configurations and local muon hopping. Our results show that muon-polaron complexes in Fe₂O₃ significantly influence the μ SR signals, demonstrating that in order to relate experimental data to intrinsic magnetic properties, both muon and polaron dynamics have to be considered. Finally, the muon-polaron complex dissociates above ~ 200 K, strongly suggesting that analogous H centers may act as electron donors.

α -Fe₂O₃ has the corundum structure (space group $R\bar{3}c$), is weakly ferromagnetic below $T_N = 948$ K, and becomes antiferromagnetic below the Morin temperature $T_M \sim 260$ K, with spins aligning pairwise antiparallel along the rhombohedral 111 axis (\hat{c} axis) [Fig. 1, inset 1]. Focusing on $T < T_M$, we carried out μ SR experiments at $2.2 < T < 265$ K in zero external magnetic field (ZF) in the LAMPF spectrometer at TRIUMF (Canada). Spin polarized, positively charged muons were implanted into a natural single crystal (SurfaceNet, Germany), with the initial muon polarization aligned within 5° normal to the \hat{c} axis. The subsequent muon decay (lifetime $\tau_\mu = 2.2 \mu$ s) enabled the observation of the time evolution of its spin polarization via the anisotropic emission of the decay positrons [32]. Due to spin precession in local magnetic fields \mathbf{B}_i from ordered Fe moments surrounding various muon stopping sites, up to three coherent oscillation frequencies $f_i = \gamma_\mu/2\pi \cdot |\mathbf{B}_i|$ were observed, where $i = 1-3$ labels the signal components and $\gamma_\mu = 2\pi \cdot 135.5$ MHz/T is the muon gyromagnetic ratio [Fig. 1 (a)]. f_1 (\bullet) is

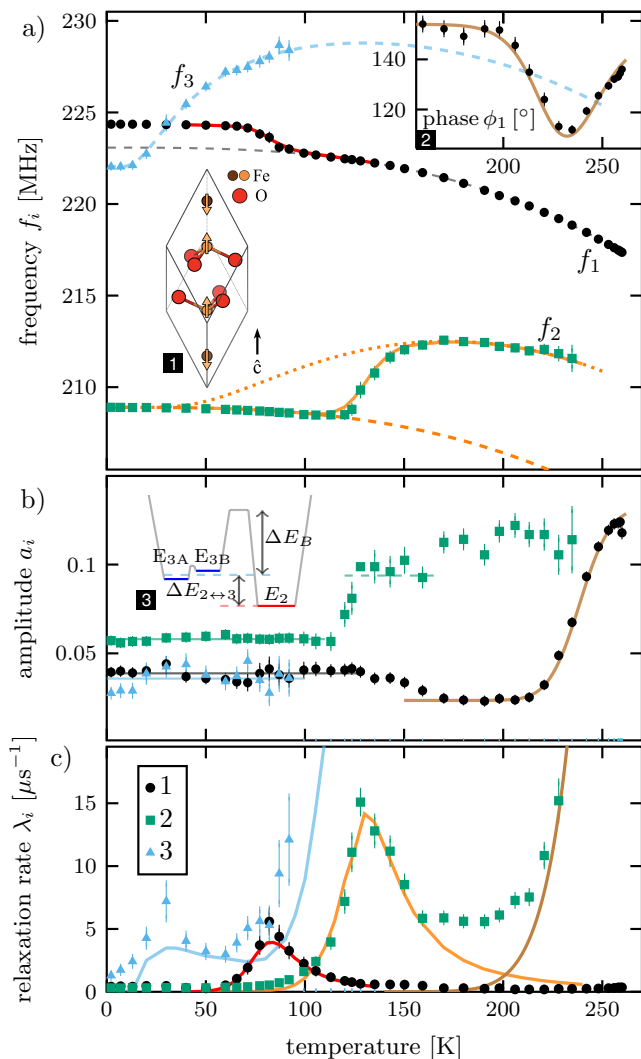


FIG. 1. Results of fits of the ZF- μ SR spectra to up to three oscillatory components $S_i(t)$ [Eqn. (1)], with $i = 1$ (\bullet), 2 (\blacksquare), 3 (\blacktriangle). Solid and dashed lines represent models as described in the main text. (a) frequencies f , (b) amplitudes a and (c) relaxation rates λ . Insets: (1) Primitive unit cell of Fe₂O₃. (2) Phase shift ϕ_1 . (3) Proposed schematic energy landscape of the muon sites associated with f_2 and f_3 (not to scale).

detected at all T up to T_M , whereas f_2 (\blacksquare) and f_3 (\blacktriangle) are only observed up to 235 K and 90 K, respectively, indicating that each f_i originates from sites that are energetically inequivalent. The spectra are fit to a sum of exponentially damped oscillatory signal components $S_i(t)$

$$S_i(t) = a_i \cos(2\pi f_i t + \phi_i) \exp(-\lambda_i t), \quad (1)$$

where a_i , f_i , ϕ_i and λ_i are the signal amplitude, frequency, phase shift and relaxation rate, respectively. Remarkably, none of the frequencies simply decrease with increasing T as they would if they followed the magnetic order parameter [41]. Instead, they display distinct step-

like features. Likewise, the amplitudes and relaxation rates vary strongly with T [Fig. 1 (b) and (c)]. In the following, we explain the data by considering muon diffusion, site transitions and charge-neutral complexes.

First, we discuss the most stable signal, S_1 [Fig. 1 (\bullet)], which we attribute to the positive charge state. The discontinuity around 80 K in f_1 is explained in terms of local hopping on a ring of adjacent, electrostatically equivalent sites [Fig. 2 (a)]. This was also observed in isomorphous Cr₂O₃ [31] and has been proposed for Fe₂O₃ [34–36]. In Cr₂O₃, the magnetic structure ($\uparrow\downarrow\uparrow\downarrow$) breaks the inversion symmetry ($\mathbf{B}(\mathbf{r}) = -\mathbf{B}(-\mathbf{r})$) such that sufficiently fast local hopping leads to a complete cancellation of the internal field and subsequent loss of the oscillatory signal, while in Fe₂O₃ ($\downarrow\uparrow\uparrow\downarrow$), $\mathbf{B}(\mathbf{r}) = \mathbf{B}(-\mathbf{r})$, and fast hopping only causes a cancellation of the radial in-plane component ($\perp \hat{c}$) [34], resulting in the drop in f_1 and the peak in λ_1 around 80 K. Our simulation of the muon polarization function [31, 42] based on (1) a simple parametrization $L(T)$ of the T -dependence of the order parameter [43] [Fig. 1 (a), gray dashed line] and (2) assuming local hopping between adjacent sites with Arrhenius-like activation (using an activation energy $E_1 = 55$ meV, prefactor $A_1 = 2 \times 10^{12}$ Hz and angle $\theta_1 = \angle(\mathbf{B}_1, \hat{c}) = 6.1^\circ$) yields good agreement (solid red lines) with the step in f_1 and shape, position and magnitude of the peak in λ_1 .

We attribute the remaining two signals, S_2 and S_3 , to charge-neutral muon states, a scenario supported by DFT as outlined below. We analyze their more complex behavior with the simplifying assumptions that (1) the internal fields causing precession at f_2 and f_3 are oriented along the \hat{c} axis, and (2) at a given site, the internal field follows $L(T)$. We propose that the unusual increase of f_3 with increasing T is due to a thermally excited state with frequency f_{3B} . At 2.2 K, only the ground state with $f_{3A} = 222.1$ MHz is occupied, however, with rising T , the excited state becomes populated, with the mean occupation probability described by the energy difference $\Delta E_3 = E_{3B} - E_{3A}$ and a Boltzmann factor $P_{E_3}(T) = e^{(-\Delta E_3/k_B T)} / [1 + e^{(-\Delta E_3/k_B T)}]$ [28], leading to a mean frequency $f_3(T) = [(1 - P_{E_3}(T))f_{3A} + P_{E_3}(T)f_{3B}] \cdot L(T)$. For $f_{3B} = 241.7 \pm 1.0$ MHz and $\Delta E_3 = 5.4 \pm 1.0$ meV, this expression yields good agreement with the data [Fig. 1 (a), dashed blue line], and allows for a prediction of the expected T -dependence beyond the temperatures where it is observed. The peak in λ_3 around 30 K is consistent with the proposed $f_{3A} \leftrightarrow f_{3B}$ transitions and indicates the presence of a small energy barrier ~ 5 meV.

Next, we address the disappearance of f_3 above 100 K, the upturn in f_2 above 120 K, and the increase in a_2 . We propose that approaching 100 K from below, muons initially in f_3 are able to overcome a barrier ΔE_B and start to transition into the lower-energy f_2 state, causing f_3 to vanish. With further increasing T , the reverse transition from f_2 to f_3 also becomes accessible on the scale of τ_μ , resulting in a dynamic joint state of f_2 and

f_3 [blue and orange dashed lines] with combined amplitude, increased relaxation and increasing (occupation-averaged) frequency [Fig. 1 (b), inset 3]. Finally, above ~ 160 K, the transition rate in both directions is sufficiently fast that a Boltzmann distribution is established, since ΔE_B , which suppresses transitions at lower T , is no longer relevant. We model the data in two steps. First, the data above 170 K is fit to a Boltzmann weighted frequency $\bar{f}_{23}(T) = [(1 - P_{E23}(T))f_2 + P_{E23}(T)f_3(T)]$ [dotted orange line], from which $\Delta E_{2\leftrightarrow 3} = E_3 - E_2 = 16.5 \pm 2.0$ meV is obtained. Then, ΔE_B is taken into account by simulating the muon polarization assuming a thermally activated $f_2 \leftrightarrow f_3$ transition with energy barrier $\Delta E_B = 95 \pm 25$ meV and prefactor $A_{23} = 4.5 \times 10^{11}$ Hz, yielding excellent agreement with the frequency step and the associated peak in λ_2 [Fig. 1, solid orange lines].

Lastly, we address the pronounced dip in the phase ϕ_1 [Fig. 1 (a), inset 2], the increase in a_1 , the disappearance of f_2 , and the sharp increase in λ_2 , all occurring around 225 K. Together, the features are clear evidence for a thermally activated transition of muons from f_2 to f_1 . Assuming a transition rate of the form $\Lambda(T) = A_{2\rightarrow 1} \exp(-\Delta E_{2\rightarrow 1}/k_B T)$, the data are consistently described [Fig. 1, brown lines] using a simple transition model [[44], Eqs. C1-C4 in Ref. [31]] with shared parameters $\Delta E_{2\rightarrow 1} = 0.35 \pm 0.05$ eV and $A_{2\rightarrow 1} = 6 \times 10^{14}$ Hz.

With that, all the major features in Fig. 1 are explained in terms of local muon hopping, thermally accessible excited states, dynamic population of metastable states separated by a barrier, and, finally, a transition of metastable f_2 states to the apparent ground state f_1 .

Now we turn to DFT to search for muon stopping sites consistent with the observed behavior. LDA+U calculations were carried out using VASP [45–48]. The μ^+ was modeled as a H nucleus, embedded within an 80-atom $2 \times 2 \times 2$ rhombohedral supercell. A site search procedure similar to Ref. 31 was carried out for both the positive and neutral charge states; additionally, negatively charged states were considered [details and structure files in [49]]. For each energetically distinct candidate site (C) [50], the precession frequency f_{dft} in the combined hyperfine and dipolar fields was calculated [Table I]. A single stable candidate site for the positive charge state (C^+), four possible sites for the charge-neutral state (C_1^0 - C_4^0) and two configurations for the negative charge state (C_1^- & C_2^-) were obtained, all with the muon stopping ~ 1 Å away from an oxygen. Independent of the charge state, the muon localizes close to the electrostatic potential minimum of the undistorted cell [Fig. 2 (a), blue isosurface]. Note that despite rapid transitions between different sites, the muon does not leave the confinement of *one* such “muon cage” bounded by two 60° rotated oxygen triangles - a site change to an adjacent cage would result in a sign change of the local \mathbf{B} , leading to a cancellation of internal field and subsequent signal loss, which is not observed for $T < T_M$ [51].

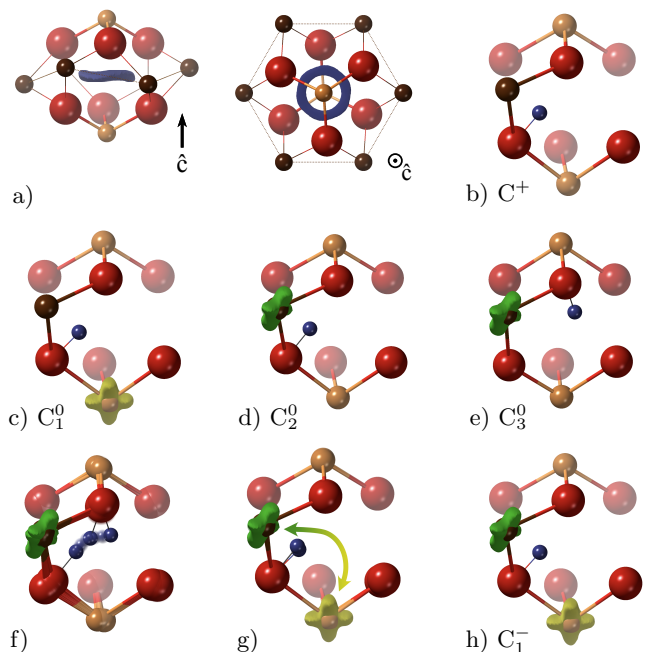


FIG. 2. Candidate muon stopping sites identified using DFT. O (red), muon (blue), Fe (light / dark brown, shade indicating opposite spin direction). (a) visualization of a “muon cage”, with the blue isosurface indicating the electrostatic minimum of the *undistorted* structure. (b) calculated site for the positive charge state C^+ . (c)-(e) charge-neutral muon-polaron complexes in three different configurations. Isosurface of the spin density of topmost occupied level on the Fe ion where the polaron predominately localizes (yellow / green indicate opposite spin). Transition between (f) C_1^0 and C_3^0 and (g) C_1^0 and C_2^0 . (h) Negative charge candidate site C_1^- with two polarons associated with the oxygen-bound muon.

We associate S_1 , the only signal observed up to T_M , with C^+ [Fig. 2 (b)], in good agreement with $f_{\text{dft}}^{C^+}$. Additionally, in analogy with Cr_2O_3 [E3 in Ref. 31], the close proximity of adjacent electrostatically equivalent sites strongly supports the T -dependence of f_1 being due to positive muons undergoing locally restricted motion within a given muon cage.

In μSR studies of magnetic materials, usually only the positive charge state is considered. However, it is clear that in Fe_2O_3 , as in Cr_2O_3 [31], the single C^+ site can not explain the data and other charge states have to be taken into account. The neutral C_1^0 - C_4^0 can be characterized as muon-polaron complexes: the bound electron predominantly localizes on a nearby Fe ion to form a small polaron, occupying an empty minority spin t_{2g} orbital and changing the Fe valence from Fe^{3+} ($3d^5$) to Fe^{2+} ($3d^6$) [Fig. 2 (c)-(e)]. The electron localization is aided by the presence of the positive muon bound to an adjacent oxygen, forming an overall charge-neutral muon-polaron complex $\text{Fe}^{2+}(\text{O}\mu)^-$ [52]. In contrast to non-magnetic materials, the spin of the bound electron is strongly coupled to the unpaired $3d$ electrons of the Fe host; as a re-

CS	Site	f_{dft} [MHz]	θ [°]	ΔE [meV]	f_{exp} [MHz]
+	C^+	228.0	7.6	0	224.4 (f_1)
0	C_1^0	214.5	8.5	0	208.9 (f_2)
	C_2^0	225.9	7.3	12.5	222.0 (f_{3A})
	C_3^0	239.5	7.1	37.2	241.7 (f_{3B})
	C_4^0	259.1	6.7	50.6	
-	C_1^-	225.3	7.9	0	
	C_2^-	211.0	8.7	3.7	

TABLE I. Candidate muon stopping sites C obtained with DFT for the positive, neutral and negative charge states (CS): calculated precession frequencies f_{dft} , angle $\theta = \angle(\mathbf{B}_i, \hat{c})$ and energy ΔE relative to the ground state of each charge state. f_{exp} lists observed frequencies next to proposed sites.

sult, the spin degree of freedom typical of paramagnetic Mu centers is lost, and only a single frequency rather than the characteristic multiplet is displayed.

In a given muon cage, there are two distinct Fe positions belonging to different magnetic sublattices: axially above and below [Fig. 2(a), light brown], or equatorially around the cage in a buckled plane [Fig. 2(a), dark brown]. Each of the equatorial Fe is bound to two oxygens that make up the cage, with one bond slightly longer than the other. Focusing on the three lowest-energy C^0 sites, C_1^0 - C_3^0 differ in both the position of muon and polaron: for C_1^0 , the electron is predominantly localized on an axial Fe [Fig. 2(c)], whereas for C_2^0 and C_3^0 , the polaron is mainly on an equatorial Fe, with the muon bound either to the oxygen forming the long (C_2^0) [Fig. 2(d)] or the short (C_3^0) bond [Fig. 2(e)]. We propose that C_1^0 - C_3^0 can explain the S_2 and S_3 signals as follows: transitions between C_2^0 and C_3^0 mainly correspond to the muon hopping between the two oxygens that are both bound to the Fe^{2+} (polaron) ion [Fig. 2(f)]. Noting that the presence of the extra electron significantly distorts the lattice and decreases the distance and thus the barrier between the two sites, this provides a plausible mechanism for the low- T dynamics ($f_{3A} \leftrightarrow f_{3B}$), and renders C_2^0 and C_3^0 good candidate sites for f_{3A} and f_{3B} , jointly explaining S_3 . C_1^0 is assigned to S_2 , supported by its low energy and good agreement in measured and calculated frequency. Given the uncertainties inherent to DFT [53], there is good agreement between DFT and all observed frequencies [Table I]. Considering the proposed $f_2 \leftrightarrow f_3$ transitions, this state assignment suggests that for $T > \sim 100$ K, transitions between C_1^0 and C_2^0 occur, implying that *polaron* dynamics rather than muon hopping drives this dynamic process [Fig. 2(g)]. The energy barrier $\Delta E_B \approx 95 \pm 25$ meV is attributed to both the small polaron hopping (aided by the presence of the muon for the two Fe ions involved) and a spin contribution (of the order of $\sim k_B T_N = 82$ meV [54]), accounting for the polaron hopping between magnetic sublattices. Note that the energies of C_1^0 and C_2^0 are very close [Table I], en-

abling the back-*and*-forth transitions postulated above, with the energy difference matching closely $\Delta E_{2 \leftrightarrow 3}$. In sharp contrast, the different complex configurations in Cr_2O_3 are well separated in energy [31], and neither unusual dynamics, nor frequencies deviating from the order parameter are observed. The difference in energy separation (and consequently, dynamic behavior) is attributed to the strength of the polaron-induced Jahn-Teller (JT) distortion [55]; Cr^{2+} with $3d^4$ (high spin) is strongly JT-active, whereas Fe^{2+} with $3d^6$ (high spin) is only weakly JT-active.

Lastly, we discuss the negative (C^-) charge state, comprised of an oxygen-bound muon and *two* polarons, located on both axial and equatorial Fe ions [C_1^- shown in Fig. 2(h)]. DFT in large (270-atom) supercells suggest that C_1^- is lower in energy than C_1^0 and a separated polaron; likewise, C_1^0 is lower in energy than C^+ and a separated polaron [49], indicating that C^- is the lowest energy state *if* sufficient excess electrons are available. Also, $f_{\text{dft}}^{C_1^-}$ is close to f_1 , rendering C_1^- an alternative candidate for S_1 . However, we consider the scenario where S_1 originates from C_1^- rather than C^+ unlikely, since (1) at low T , polarons are highly immobile, and while it is conceivable (and necessary to explain the data) that a thermalizing muon captures a single electron, it is implausible that all other muons capture two electrons to form C^- and no C^+ is formed at all. (2) Above 250 K, S_1 represents the complete signal, and while the Boltzmann factor favors C^- , the overwhelming degeneracy of free polaron states away from the muon is expected to dominate. Thus, we are confident in assigning S_1 to C^+ .

This assignment directly implies that the $f_2 \rightarrow f_1$ transition around 225 K corresponds to a charge-state transition from neutral to positive, which we characterize as a complex dissociation [30], i.e. a separation of the polaron and the oxygen-bound muon, rather than an ionization of the bound electron to the conduction band. Then, $\Delta E_{2 \rightarrow 1} \approx 0.35$ eV corresponds to the barrier the polaron has to overcome to dissociate from the positive muon. Notably, $\Delta E_{2 \rightarrow 1}$ is larger than barrier estimates of 0.1–0.2 eV for “free” polaron hopping [10, 14, 18–20], indicating that the muon acts as a trap and thus lowers polaron mobility [20]. By the well established analogy between μ^+ and a proton [24–27], these results indicate that isolated H impurities in Fe_2O_3 form corresponding $\text{Fe}^{2+}(\text{OH})^-$ complexes. While the dynamic behavior, especially at low T , is expected to be different owing to the mass difference ($m_\mu \approx \frac{1}{9} m_p$), the electronic structure (which depends on the *reduced* electron mass) is virtually identical. Likewise, the observed complex dissociation, characterized by the *polaron* hopping away, is expected to be comparable for H-polaron complexes, suggesting that at room temperature, interstitial H contributes “free” polarons and thus increases the carrier density, while simultaneously acting as a trap, decreasing overall carrier

mobility.

In summary, we present a detailed μ SR study of Fe_2O_3 , and consistently explain the observed spectra by considering charge-neutral muon-polaron complexes, with different complex configurations providing an intuitive explanation for magnetically distinct sites that are close in energy. The unusual T -dependences of the observed frequencies and relaxation rates are well described by transitions between these complex configurations, demonstrating that the presence of muon-polaron complexes in magnetic materials can alter the observed μ SR signals such that they not only reflect the intrinsic magnetic properties, but also both muon and polaron dynamics. The identification of charge-neutral $\text{Fe}^{2+}(\text{O}\mu)^-$ [52] complexes clearly shows that Cr_2O_3 , the first magnetic material where muon-polaron complexes were observed [31], is not an isolated case. Analogous complexes with similarly inconspicuous signals likely exist in other insulating magnets, in particular in TMOs where the multivalent character of the TM ions facilitates polaron formation. We contend that a careful consideration of such charge-neutral muon states (and associated local dynamics, as demonstrated here), in conjunction with DFT, can significantly enhance the muon's power as a sensitive local probe of magnetism. Lastly, the presence of polaronic muon centers suggests that H impurities form analogous $\text{Fe}^{2+}(\text{OH})^-$ complexes at low T , but dissociate at room temperature, indicating that interstitial H in Fe_2O_3 increase the charge carrier density while simultaneously lowering the polaron mobility.

This research was performed at the TRIUMF Centre for Materials and Molecular Science. The authors thank R. Abasalti and D. Vyas for excellent technical support, and M. Berciu and R. C. Vilao for stimulating discussions. Financial support came from a NSERC Discovery grant to R.F.K. MHD acknowledges support from a SBQMI QuEST Fellowship. JKS and NAS acknowledge funding from the European Research Council (ERC) under the European Union's Horizon 2020 research and innovation programme grant agreement No 810451. Computational resources were provided by ETH Zürich and the Swiss National Supercomputing Centre, project ID s889.

* MHD and JKS contributed equally to this work.

- [1] F. J. Morin, *Phys. Rev.* **78**, 819 (1950).
- [2] C. G. Shull, W. A. Strauser, and E. O. Wollan, *Phys. Rev.* **83**, 333 (1951).
- [3] S. Lany, *J. Phys. Condens. Matter* **27**, 283203 (2015).
- [4] F. P. Chmiel, N. Waterfield Price, R. D. Johnson, A. D. Lamirand, J. Schladt, G. van der Laan, D. T. Harris, J. Irwin, M. S. Rzechowski, C.-B. Eom, and P. G. Radaelli, *Nat. Mater.* **17**, 581 (2018).
- [5] D. L. Cortie, T. Buck, M. H. Dehn, V. L. Karner, R. F. Kiefl, C. D. P. Levy, R. M. L. McFadden, G. D. Morris, I. McKenzie, M. R. Pearson, X. L. Wang, and W. A. MacFarlane, *Phys. Rev. Lett.* **116** (2016), 10.1103/PhysRevLett.116.106103.
- [6] A. Sanson, I. Kantor, V. Cerantola, T. Irifune, A. Carnera, and S. Pascarelli, *Phys. Rev. B* **94** (2016), 10.1103/PhysRevB.94.014112.
- [7] S. Xu, A. H. Habib, S. H. Gee, Y. K. Hong, and M. E. McHenry, *J. Appl. Phys.* **117**, 17A315 (2015).
- [8] D. A. Grave, N. Yatom, D. S. Ellis, M. C. Toroker, and A. Rothschild, *Adv. Mater.* **30**, 1706577 (2018).
- [9] J. Zhang and S. Eslava, *Sustain. Energy Fuels* **3**, 1351 (2019).
- [10] E. Pastor, J.-S. Park, L. Steier, S. Kim, M. Grätzel, J. R. Durrant, A. Walsh, and A. A. Bakulin, *Nat. Commun.* **10** (2019), 10.1038/s41467-019-11767-9.
- [11] L. M. Carneiro, S. K. Cushing, C. Liu, Y. Su, P. Yang, A. P. Alivisatos, and S. R. Leone, *Nat. Mater.* **16**, 819 (2017).
- [12] J. Husek, A. Cirri, S. Biswas, and L. R. Baker, *Chem. Sci.* **8**, 8170 (2017).
- [13] A. Kay, M. Fiegenbaum-Raz, S. Müller, R. Eichberger, H. Dotan, R. de Krol, F. F. Abdi, A. Rothschild, D. Friedrich, and D. A. Grave, *Adv. Funct. Mater.* , 1901590 (2019).
- [14] K. M. Rosso, D. M. A. Smith, and M. Dupuis, *J. Chem. Phys.* **118**, 6455 (2003).
- [15] N. Iordanova, M. Dupuis, and K. M. Rosso, *J. Chem. Phys.* **122**, 144305 (2005).
- [16] J. Lee and S. Han, *Phys. Chem. Chem. Phys.* **15**, 18906 (2013).
- [17] A. J. E. Rettie, W. D. Chemelewski, D. Emin, and C. B. Mullins, *J. Phys. Chem. Lett.* **7**, 471 (2016).
- [18] A. J. E. Rettie, W. D. Chemelewski, B. R. Wygant, J. Lindemuth, J.-F. Lin, D. Eisenberg, C. S. Brauer, T. J. Johnson, T. N. Beiswenger, R. D. Ash, X. Li, J. Zhou, and C. B. Mullins, *J. Mater. Chem. C* **4**, 559 (2016).
- [19] B. Zhao, T. C. Kaspar, T. C. Droubay, J. McCloy, M. E. Bowden, V. Shutthanandan, S. M. Heald, and S. A. Chambers, *Phys. Rev. B* **84** (2011), 10.1103/PhysRevB.84.245325.
- [20] T. J. Smart and Y. Ping, *J. Phys. Condens. Matter* **29**, 394006 (2017).
- [21] A. Shluger, in *Handbook of Materials Modeling*, edited by W. Andreoni and S. Yip (Springer International Publishing, Cham, 2019) pp. 1–22.
- [22] S. J. Pearton, J. W. Corbett, and T. S. Shi, *Appl. Phys. Solids Surf.* **43**, 153 (1987).
- [23] C. G. Van de Walle and J. Neugebauer, *Nature* **423**, 626 (2003).
- [24] K. Chow, B. Hitti, and R. Kiefl, in *Semiconductors and Semimetals*, Vol. 51 (Elsevier, 1998) pp. 137–207.
- [25] S. F. J. Cox, J. S. Lord, S. Cottrell, J. M. Gil, H. V. Alberto, A. Keren, D. Prabhakaran, R. Scheuermann, and A. Stoykov, *J. Phys. Condens. Matter* **18**, 1061 (2006).
- [26] S. F. J. Cox, J. L. Gavartin, J. S. Lord, S. P. Cottrell, J. M. Gil, H. V. Alberto, J. P. Duarte, R. C. Vilão, N. A. de Campos, D. J. Keeble, E. A. Davis, M. Charlton, and D. P. van der Werf, *J. Phys. Condens. Matter* **18**, 1079 (2006).
- [27] S. F. J. Cox, *Rep. Prog. Phys.* **72**, 116501 (2009).
- [28] R. C. Vilão, R. B. L. Vieira, H. V. Alberto, J. M. Gil, A. Weidinger, R. L. Lichti, B. B. Baker, P. W. Mengyan, and J. S. Lord, *Phys. Rev. B* **92**, 081202(R) (2015).

- [29] K. Shimomura, R. Kadono, A. Koda, K. Nishiyama, and M. Mihara, Phys. Rev. B **92**, 075203 (2015) (2015).
- [30] T. U. Ito, W. Higemoto, A. Koda, and K. Shimomura, Appl. Phys. Lett. **115**, 192103 (2019).
- [31] M. H. Dehn, J. K. Shenton, S. Hohenstein, Q. N. Meier, D. J. Arseneau, D. L. Cortie, B. Hitti, A. C. Y. Fang, W. A. MacFarlane, R. M. L. McFadden, G. D. Morris, Z. Salman, H. Luetkens, N. A. Spaldin, M. Fechner, and R. F. Kiefl, Phys. Rev. X **10** (2020), 10.1103/PhysRevX.10.011036.
- [32] A. Yaouanc and P. Dalmas de Réotier, *Muon Spin Rotation, Relaxation, and Resonance* (Oxford University Press, 2011).
- [33] P. Dalmas de Réotier, A. Maisuradze, and A. Yaouanc, J. Phys. Soc. Jpn. **85**, 091010 (2016).
- [34] H. Graf, W. Hofmann, W. Kündig, P. F. Meier, B. D. Patterson, W. Reichhart, and A. Rodriguez, Hyperfine Interact. **4**, 452 (1978); H. Graf, W. Hofmann, W. Kündig, P. F. Meier, B. D. Patterson, and A. Rodriguez, Solid State Commun. **25**, 1079 (1978).
- [35] C. Boekema, K. Rüegg, and W. P. Hofmann, Hyperfine Interact. **8**, 609 (1981).
- [36] K. C. B. Chan, R. L. Lichti, C. Boekema, A. B. Denison, D. W. Cooke, and M. E. Schillaci, Hyperfine Interact. **31**, 481 (1986); K. B. Chan, *Localization and Local Motion of Muons in Antiferromagnetic Oxides: Vanadium Oxide and Iron Oxide*, MSc thesis, Texas Tech University (1986); K. C. Chan, *Muon Sites in Transition Metal Oxides*, PhD thesis, Texas Tech University (1988).
- [37] K. Rüegg, C. Boekema, W. Hofmann, W. Kündig, and P. F. Meier, Hyperfine Interact. **6**, 99 (1979).
- [38] K. Rüegg, C. Boekema, A. Denison, W. Hoffmann, and W. Kündig, J. Magn. Mater. **15-18**, 669 (1980).
- [39] K. J. Rüegg, C. Boekema, W. Kündig, P. F. Meier, and B. O. Patterson, Hyper Fine Interact. **8**, 547 (1981).
- [40] C. Boekema, A. B. Denison, and K. J. Rüegg, J. Magn. Mater. **36**, 111 (1983).
- [41] F. van der Woude, Phys. Status Solidi B **17**, 417 (1966).
- [42] M. H. Dehn, D. G. Fleming, W. A. MacFarlane, M. J. MacLachlan, V. M. Zamarion, and R. F. Kiefl, Proc 14th Int Conf Muon Spin Rotat. Relax. Reson. J. Phys. Soc. Jpn. **21**, 011032 (2018).
- [43] $L(T) = (1 - (T/T_c)^\alpha)^\beta$, with $T_c = 948$ K. Fitting $f_1^L(T) = f_1^* \cdot L(T)$ to f_1 data in the range 105–250 K yields $\alpha = 2.92$, $\beta = 1.13$ and $f_1^* = 223.08$ MHz [Fig. 1 (a), gray dashed line].
- [44] P. F. Meier, Phys. Rev. A **25**, 1287 (1982).
- [45] G. Kresse and J. Hafner, Phys. Rev. B **47**, 558 (1993).
- [46] G. Kresse and J. Hafner, Phys. Rev. B **49**, 14251 (1994).
- [47] G. Kresse and J. Furthmüller, Phys. Rev. B **54**, 11169 (1996).
- [48] G. Kresse and D. Joubert, Phys. Rev. B **59**, 1758 (1999).
- [49] J. K. Shenton, *Supplementary Material Containing DFT Structure Files and Convergence Tests for our μ SR study on Fe_2O_3* , <http://doi.org/10.5281/zenodo.3985400> (2020).
- [50] By symmetry, each site is part of an ensemble of six electrostatically equivalent sites per unit cell.
- [51] Long range muon diffusion in Fe_2O_3 leading to signal cancellation *does* occur [34], however only above ~ 400 K.
- [52] Charge-neutral relative to $Fe^{3+}O^{2-} + \mu^+$, i.e. the additional charge from the muon is compensated.
- [53] The need to choose a Hubbard U_{eff} ($U_{\text{eff}} = 4$ eV for results above) is the dominant source of uncertainty. Varying U_{eff} between 3–6 eV, we find that although the numerical values vary as a function of U_{eff} , the qualitative behavior remains robust throughout 3–5 eV, the range typically employed for Fe d states (see [49]).
- [54] D. Emin and N. L. H. Liu, Phys. Rev. B **27**, 4788 (1983).
- [55] H. A. Jahn and E. Teller, Proc Roy Soc A **161**, 16 (1937).